J. Electrochem. Sci. Eng. **15(5)** (2025) 2711; http://dx.doi.org/10.5599/jese.2711

Open Access : : ISSN 1847-9286
https://pub.iapchem.org/ojs/index.php/JESE

Original scientific paper

Polyarginine decorated zinc oxide carbon nanotube composite sensor for the voltammetric detection of ferulic acid and hydroquinone

Karnayana. P. Moulya and Jamballi G. Manjunatha✉

[1]*Department of Chemistry, FMKMC College, Madikeri, Constituent College of Mangalore University, Karnataka, India*

Corresponding author: ✉ *manju1853@gmail.com, Tel: +91-0827222833*

Received: March 13, 2025; Accepted: July 3, 2025; Published: July 14, 2025

Abstract

In the present work, the electrochemical detection of ferulic acid (FA) was done using zinc oxide (ZnO) prepared by the application of the green synthesis method in combination with carbon nanotube modified with arginine (PAG/ZnO-CNTCE). X-ray diffraction, scanning electron microscopy, electrochemical impedance spectroscopy and energy-dispersive X-ray spectroscopy were applied for the morphological and structural analysis of prepared ZnO nanoparticles, ZnO carbon nanotube composite electrode (ZnO-CNTCE), and polyarginine modified electrode, PAG/ZnO-CNTCE. Cyclic voltammetry (CV) and linear sweep voltammetry (LSV) were successfully applied for electrochemical characterization and sensitive detection of FA under optimum conditions of pH, accumulation time, accumulation potential, and scan rate with the transfer of two electrons and two protons. The limit of detection of 0.08 and 0.404 µM, respectively, was obtained for CV and LSV in the wide range of 0.4 to 10.0 µM and 0.2 to 10.0 µM. The limit of quantification was found to be 0.274 and 1.348 µM for CV and LSV. The simultaneous analysis confirmed the selectivity of the electrode towards FA in the presence of hydroquinone at two different potentials. The developed PAG/ZnO-CNTCE exhibited excellent reproducibility, stability, repeatability, and anti-interferent properties. FA was successfully detected at the surface of PAG/ZnO-CNTCE with an impressive recovery rate for both popcorn and corn powder samples.

Keywords

Antioxidant compounds; carbon nanomaterial; metal oxide nanoparticles; *Muntingia calabura* leaves; thin polymer film; corn samples

Introduction

Antioxidants play a vital role in reducing the oxidative stress caused by free radicals, which might cause cancer, cardiovascular diseases, aging, and other neurological disorders. Apart from the anti-oxidant systems present in the human body, antioxidants can be sourced through food and diet [1].

Ferulic acid (FA) is a hydroxycinnamic acid-derived phenolic compound widely found in fruits, vegetables, grains, nuts, coffee, leaves, beans, beverages, Chinese medicinal plants, *etc*. It is basically found in the cell walls of several plants, both in the esterified saccharide form and in the free form [2]. FA exhibits various properties such as antioxidant [3], anticarcinogenic [4], antiaging [5], anti-inflammatory [6], antithrombic [7], antiallergic [8], antiviral [9], anti-diabetic [10], and antimicrobial [11]. Along with these advantages, FA has other applications in cosmetics primarily in body lotions due to its UV absorber property [12], in the preservation of food due to its ability to reduce the growth of fungi and bacteria and act as a natural preservative [13], as a precursor of vanillin [14], and as an edible film for packing purposes [15]. Owing to these advantages, detection of FA has gained importance in both the food and cosmetic industries. On the other hand, hydroquinone (HQ) acts as a stabilizing agent in photographic developers, as an antioxidant, and in cosmetics for the treatment of hyperpigmentation. Therefore, simultaneous analysis of FA and HQ is necessary to detect them separately, as they may coexist.

There are several quantitative methods applied for the detection of FA, including UV-Vis spectrophotometry [16], capillary electrophoresis [17], high-performance liquid chromatography (HPLC) [18], thin layer chromatography [19], and gas chromatography [20]. However, these techniques require expensive instruments, pre-treated reagents, time, and expertise in instrument handling. To solve these complications, electrochemical sensors were introduced as a promising method for the study of FA. Various working electrodes, such as rG-CdO/MOITF/CPE [21], MgO/SWCNTs-[Bmim][Tf2N]--CPE [22], C-C_3N_4/$Li_2CoMn_3O_8$ nanocomposite [23], *etc*., were previously reported for the sensitive detection of FA. These reported works have few drawbacks, such as complicated preparation techniques, affordability, selectivity, *etc*. Therefore, suitable working material needs to be developed to overcome the barriers to the detection of FA. The sensitivity of the working electrode depends on the modifier used to enhance the performance of the electrode.

Carbon materials like graphite, graphene, carbon nanotubes (CNTs), nanostructured metals, and composites are widely used as the electrode material for electrochemical oxidation of dyes, vitamins, hormones, heavy metals, *etc*. [24-26]. CNTs are widely used for the preparation of electrodes due to their electron transfer process, which enhances the sensitivity of the electrode. They have good electrical conductivity, mechanical strength, and a large surface area to mass ratio [27,28]. Metal oxide nanoparticles, due to their properties like chemical stability, high surface area, Biocompatibility, electron transfer property, and sensitivity, are used as electrode material [29-31]. Synthesis of metal oxide through environmentally friendly green synthesis techniques has been considered a conventional method due to its sustainable approach. It uses natural sources such as fungi, bacteria, and plant extracts as the reducing agents for nanoparticle synthesis. The green synthesis approach has a wide range of applications, like affordability, retarded pollution, availability of reducing agents, and environmental conditions. Zinc oxide (ZnO) nanoparticles are one of the most widely used metal oxides in the sensing field due to their biocompatibility, wide bandgap, high adsorption ability, and fast electron transfer kinetics [32,33]. Many works have been reported for the synthesis of ZnO nanoparticles, but no one has reported the synthesis of ZnO from *Muntingia calabura* and applied it for the detection of FA.

Electropolymerized layer is one among the widely used modifiers on the surface of the electrode due to its easy preparation method and high sensitivity towards the electroactive molecules, including food dyes, antioxidants, drugs, metal ions, *etc*. [34]. Polyamino acids play a vital role in surface modification as they form stable sensing surfaces with good stability, reproducibility, and thin polymer films. Arginine (AG) has been employed as a modifier for sensing in many works

because of its conductivity and hydrophilicity properties [35]. However, AG in combination with nanomaterials has not yet been reported as a sensor for FA analysis.

The aim of the current work was to fabricate a stable sensing surface by polymerizing AG on ZnO-CNT composite surface and to study the performance of the sensor for the analysis of FA. The electrolyte pH and other electrochemical operations were optimized and finally applied for the validation of FA in real samples.

Experimental

Chemicals and reagents

Zinc nitrate hexahydrate ($Zn(NO_3)_2{\cdot}6H_2O$) (96 to 103 % purity) from Molychem, India. FA (98 % purity) from Tokyo Chemical Industry, Japan. CNT was purchased from Sisco Research Laboratory, India. Monosodium dihydrogen phosphate ($NaH_2PO_4{\cdot}H_2O$) (99.5 % purity), disodium dihydrogen phosphate ($Na_2HPO_4{\cdot}2H_2O$) (99 % purity), potassium chloride (KCl) (99.5 % purity), HQ (98 % purity), potassium ferrocyanide ($K_4[Fe(CN)_6]$), and silicone oil (90 % purity) were purchased from Nice Chemicals, India. Analytically grade chemicals were dissolved in distilled water to obtain the standard solutions and used for the investigation. FA (0.1 mM), $Zn(NO_3)_2{\cdot}6H_2O$ (0.1 M), KCl (0.1 M) and $K_4[Fe(CN)_6]$ (0.1 mM) were prepared by dissolving in distilled water.

Instrumentation and electrochemical cell

The electrochemical analysis was done using the three-electrode setup incorporated within the CHI-6038E. The ZnO carbon nanotube composite electrode (ZnO-CNTCE) and polyarginine modified carbon nanotube composite electrode (PAG/ZnO-CNTCE) functioned as the working electrodes, while the platinum electrode and saturated calomel electrode (SCE) acted as the auxiliary and reference electrodes, respectively. The supporting electrolytic solutions used for the analysis were prepared using an EQ-610 pH meter. The scanning electron microscopy (SEM), energy-dispersive X-ray spectroscopy (EDS) and X-ray diffraction (XRD) were obtained from Vignan Bhavan, Mysore, India. EIS was measured at 0.018 V, using 0.005 V amplitude of the alternating signal, and a frequency range between 1 MHz and 1 Hz.

Preparation of ZnO nanoparticles

Zinc nitrate hexahydrate solution (0.1 M) was prepared using distilled water. *Muntingia calabura* leaves extract (20 ml) was added to the above solution with constant stirring at 80 °C for 30 minutes, and the colour of the solution changed to yellow. After stirring for 30 minutes, NaOH (1 M) was added dropwise till the solution colour changed to a pale-yellow precipitate. Stirred for a few more minutes at 80 °C until full precipitation, the solution was cooled to room temperature and centrifuged. The ZnO nanoparticles obtained were collected and oven dried overnight at 70 °C. The obtained sample was calcinated in a furnace at 400 °C with 15 minutes holding time to remove the impurities. The ZnO nanoparticles obtained were used for the preparation of the electrode. The schematic representation for ZnO synthesis can be seen in Scheme 1.

Preparation of ZnO-carbon nanotube electrode

A carbon nanotube electrode (CNTCE) was fabricated by mixing carbon nanotubes and silicone oil in the proportion 60:40 using a mortar and pestle. The prepared paste was then embedded into the 3 mm cavity of the Teflon tube, and the smooth surface was obtained by gently rubbing the surface on tissue paper. The composite sensor was developed by adding 40 mg of ZnO nanoparticles to the above mixture. The prepared ZnO-CNTCE was utilized for additional studies.

Scheme 1. *Schematic illustration for the preparation of ZnO nanoparticles*

Preparation of real samples

The popcorn sample was dried, weighed, transferred into a beaker containing ethanol, and sonicated at 50 °C for 2 hours. The mixture was cooled until it reached room temperature and filtered using a Whatman paper and diluted with ethanol to attain the standard stock solution. The corn powder solution was also prepared following the above procedure and used for the analysis of FA.

Results and discussions

Structural analysis of ZnO nanoparticles

The XRD pattern for the ZnO nanoparticles prepared using *Muntingia calabura* leaf extract can be seen in Figure 1. The diffraction peaks at 2θ of 32.02, 34.64 and 36.46° corresponding to (110), (002) and (110) planes, respectively, confirm the development of ZnO with a crystalline structure.

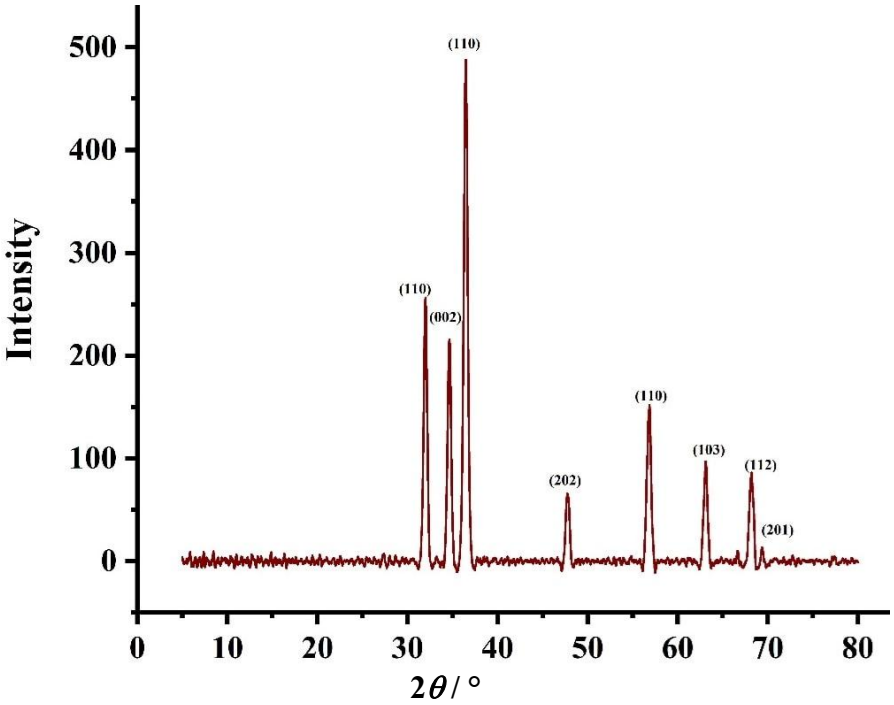

Figure 1. *XRD pattern of ZnO nanoparticles*

All the peaks obtained matched with the JCPDF Card No.36-1451. The expanded diffraction peaks are caused by the ZnO nanoparticles' refined size, which remains after 400 °C calcination. The average crystalline size (D) of the synthesized ZnO nanoparticles was calculated using Scherrer's formula, Equation (1)

$$D = \frac{K\lambda}{\beta \cos\theta} \quad (1)$$

where K is the Scherrer constant, β designates the width of the XRD peak at half height, λ is the wavelength of X-ray diffraction, and θ signifies the Bragg diffraction. The crystalline size of the synthesized ZnO particles was found to be 17.14 nm.

Energy-dispersive X-ray spectroscopy interpretation of ZnO nanoparticles

The element analysis of ZnO nanoparticles was investigated using EDS. Figure 2 shows the EDS spectrum obtained for the ZnO nanoparticles synthesized using *Muntingia calabura* leaves. The results depict that the synthesized material contains zinc and oxygen, confirming the formation of the desired nanoparticles. It was further used as the electrode material.

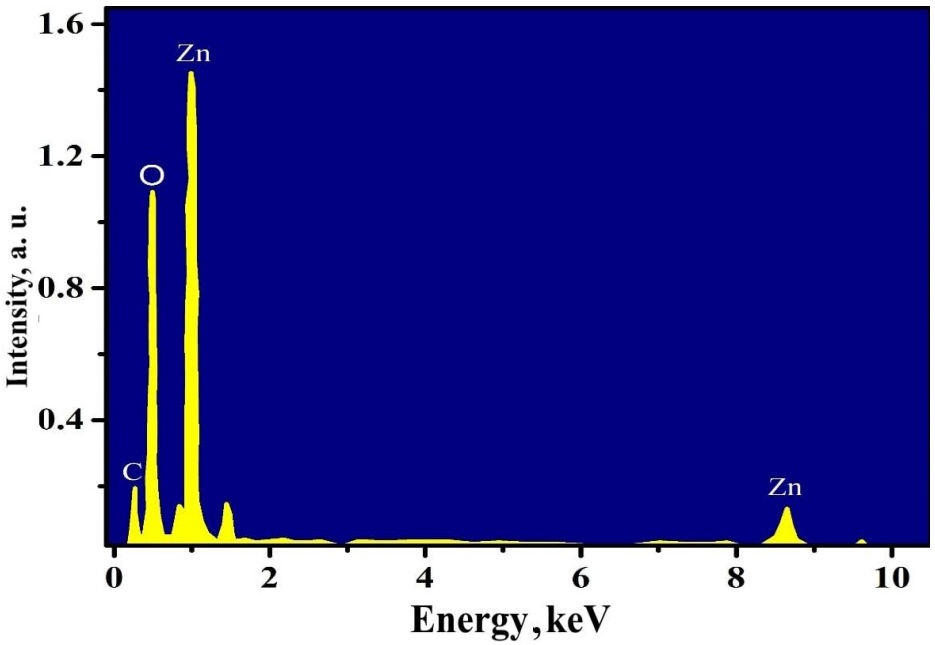

Figure 2. *EDS spectrum of ZnO nanoparticles*

Optimization of PAG/ZnO-carbon nanotube electrode formation

The electropolymerization technique was applied for the development of the polyarginine (PAG) on the surface of ZnO-CNTCE by cycling 10 potential cycles in 7.0 pH of 0.2 M phosphate buffer (PB) solution containing 1.0 mM AG for the preparation of PAG/ZnO-CNTCE. CVs for the formation of polymer can be seen in Figure 3(a). The optimization of the number of cycles was done by measuring the sensitivity of the fabricated sensor towards the detection of 0.1 mM FA. The number of cycles was increased in the interval of 5 cycles, like 5, 10, 15 and 20. It was observed that the current for 0.1 mM FA at the surface of PAG/ZnO-CNTCE increased from 5 to 10 cycles, and thereafter it was reduced until 20 cycles. As the thickness of the polymer layer increased, the working electrode lost its electrocatalytic activity. The results depicting the current response at different numbers of cycles can be seen in Figure 3(b). Given the observed enhancement after 10 cycles, these were deemed the optimal conditions for further studies.

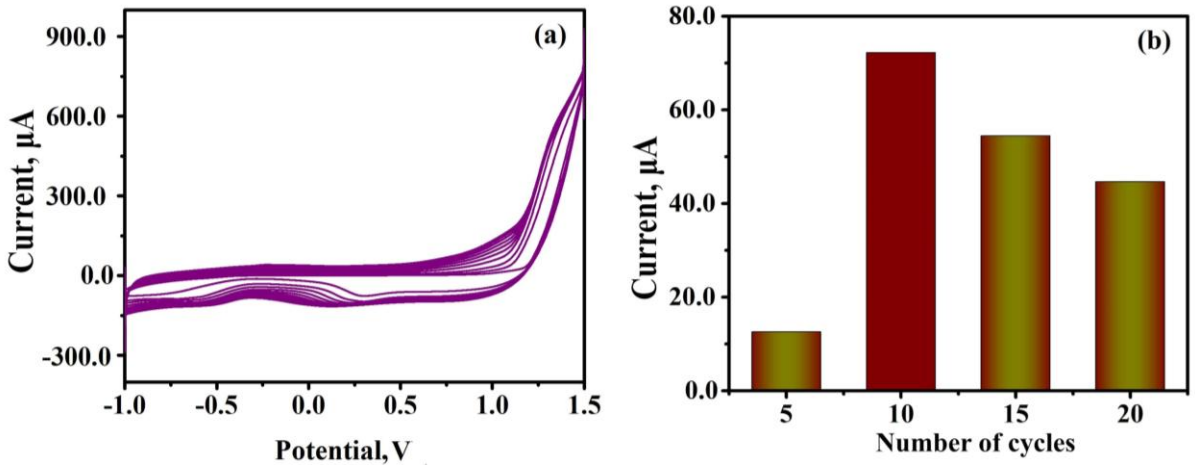

Figure 3. *(a) Electropolymerization of 1.0 mM AG on the surface of ZnO-CNTCE in 7.0 pH (0.2 M PB) in the potential window of -1.0 to 1.5 V at 0.1 V/s of scan rate; (b) graph of peak current for 0.1 mM FA oxidation against the number of cycles*

Scanning electron microscopy characterization of working electrodes

The surface modification of the fabricated electrodes was analyzed using SEM images. In Figure 4(a), the prepared ZnO nanoparticles are presented, showing a sponge-like cluster containing tube-like structures. Figure 4(b) presents the ZnO-CNTCE electrode surface, which is rough and contains irregularly shaped structures. Figure 4(c) depicts the surface of ZnO-CNTCE after electropolymerizing of AG. We can see the polymer layer covering the composite paste of ZnO and CNT. The polymer film formed is thin since we can still see the nanoparticles. The polymer film increased the active surface area of PAG/ZnO-CNTCE.

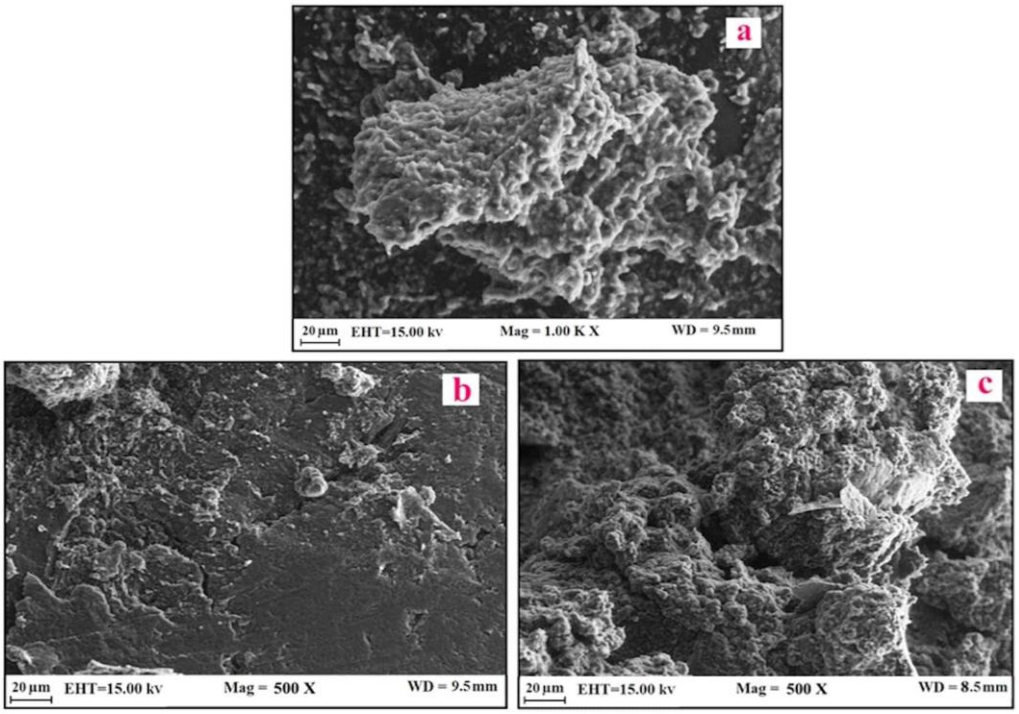

Figure 4. *SEM images of (a) ZnO nanoparticles; (b) ZnO-CNTCE; (c) PAG/ZnO-CNTCE*

Analysis of active surface area and electrochemical impedance spectroscopy

The electrochemical characteristics of the working electrodes were analysed in the redox solution (1.0 M KCl) containing 0.1 mM $K_4[Fe(CN)_6]$, at the scan rate of 0.1 V s^{-1}. Figure 5(a) displays the CVs

for the oxidation of $K_4[Fe(CN)_6]$ at ZnO-CNTCE (curve a) and PAG/ZnO-CNTCE (curve b). Due to the slow electron transfer, a small redox peak current was observed for ZnO-CNTCE, while at the surface of PAG/ZnO-CNTCE, the peak current was enhanced, possibly due to the fast electron transfer. The peak-to-peak separation (ΔE_p) for ZnO-CNTCE was 0.3857 V, and at PAG/ZnO-CNTCE, it was 0.0708 V. The decreased ΔE_p value for the PAG modified electrode validates the development of polymer film on the unmodified surface, which enhances the sensitivity of the sensor. The surface area of both ZnO-CNTCE and PAG/ZnO-CNTCE was formulated using the Randles-Ševčik equation given below as Equation (2) [37]:

$$I_p=2.65\times10^5 n^{3/2} v^{1/2} D^{1/2} CA \quad (2)$$

The active surface area was found to be 0.008 cm^2 for ZnO-CNTCE and 0.018 cm^2 for PAG/ZnO-CNTCE, respectively. These values were obtained by substituting the values of I_p representing the peak current, n representing the number of electrons transferred, v representing the scan rate, D indicating the diffusion coefficient, and C symbolizing the concentration of $K_4[Fe(CN)_6]$.

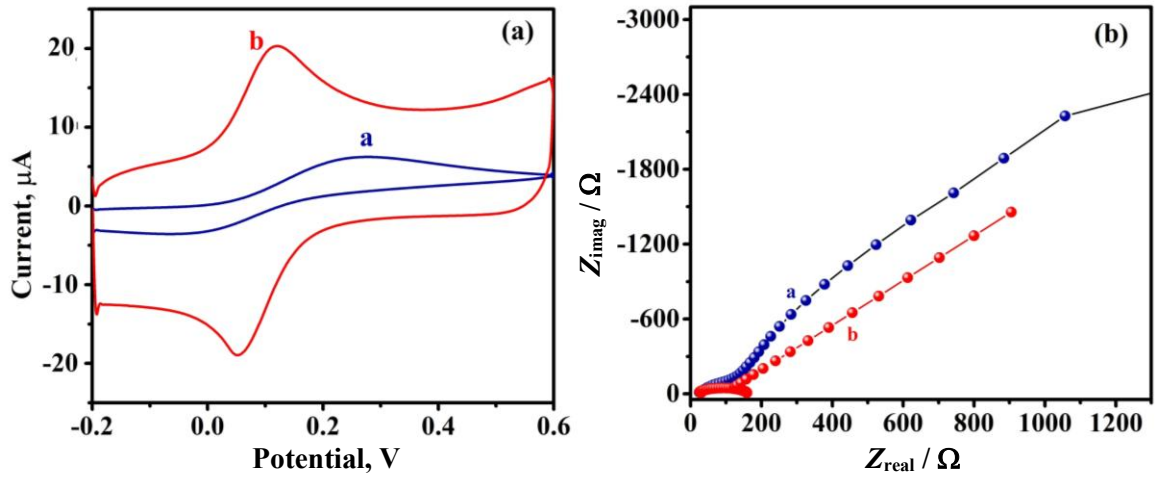

Figure 5. *(a) CVs (0.1 V/s) of 0.1 mM $K_4[Fe(CN)_6]$ in 0.1 M KCl at ZnO-CNTCE (curve a) and PAG/ZnO-CNTCE (curve b); (b) Nyquist plots for 0.1 mM $K_4[Fe(CN)_6]$ in 0.1 M KCl at ZnO-CNTCE (curve a) and PAG/ZnO-CNTCE (curve b)*

To gain information related to the charge transfer resistance (R_{ct}) for 0.1 mM $K_4[Fe(CN)_6]$ in 0.1 M KCl at the surface of both ZnO-CNTCE and PAG/ZnO-CNTCE, an EIS study was conducted. Figure 5(b) shows the Nyquist plots related to the EIS analysis containing a dominant linear part corresponding to the diffusion-controlled process at lower frequencies, while the semicircle region corresponds to the electron transfer taking place at higher frequencies. The diameter of the Nyquist plot gives the charge transfer resistance (R_{ct}) value, and R_{ct} values were 190 Ω for ZnO-CNTCE (curve a) and 119 Ω for PAG/ZnO-CNTCE (curve b), signifying the formation of a polymer film, which increases the sensitivity of the proposed electrode. The heterogeneous electron transfer rate (k_s) was found by substituting the corresponding values in Equation (3) [38].

$$k_s = RT/n^2F^2R_{ct}AC \quad (3)$$

The k_s value for ZnO/CNTCE was found to be 1.246×10^{-5} cm s^{-1}, while for PAG/ZnO-CNTCE it was 9.797×10^{-6} cm s^{-1}. The higher value obtained for the PAG modified electrode suggests that the modification promotes the transfer of electrons between the redox solution and the electrode surface.

Electrochemical response of ferulic acid at the surface of working electrodes

The redox behavior of 0.1 mM FA at 4.5 pH of 0.2 M PB was investigated at the electrode surface of both ZnO-CNTCE and PAG/ZnO-CNTCE by applying the CV method (Figure 6). The CV curves for FA at ZnO-CNTCE (curve a) showed poor redox response, while at the surface of PAG/ZnO-CNTCE (curve c), good oxidation and reduction peaks were obtained at 0.3654 V anodic peak potential (E_{pa}) and cathodic peak potential 0.3121 V (E_{pc}) with peak currents of 72.48 µA anodic peak current (I_{pa}) and 69.24 µA cathodic peak current (I_{pc}). For the absence of FA in 4.5 pH (0.2 M PB) at PAG/ZnO-CNTCE (curve b), the CV curve showed no peak response. Hence, the sensing ability of PAG/ZnO-CNTCE had a great impact on the detection of FA.

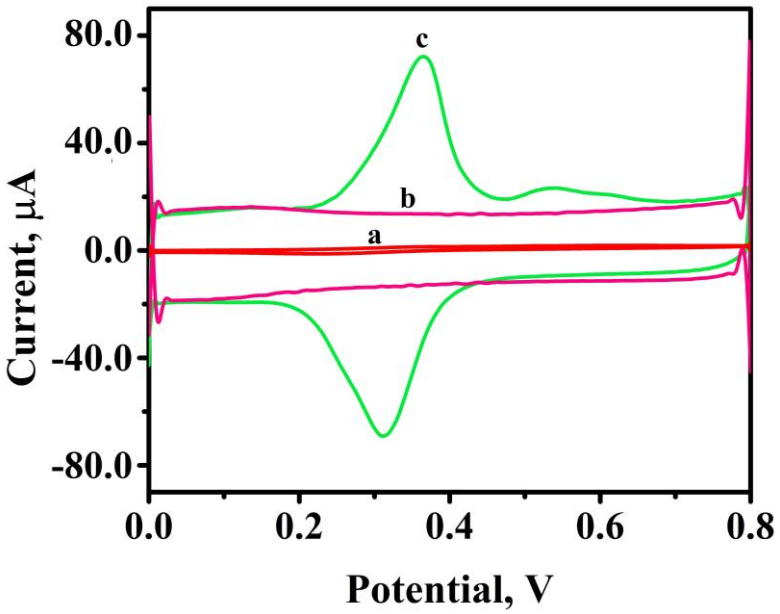

Figure 6. *CVs (0.1 Vs^{-1}) for 0.1 mM FA in 4.5 pH of 0.2 M PB at ZnO-CNTCE (curve a), PAG/ZnO-CNTCE (curve c), and for the absence of FA at PAG/ZnO-CNTCE (curve b)*

Effect of solution pH

The CV technique was implemented for studying the influence of pH of 0.2 M PB solution on electrochemical reaction of 0.1 mM FA in the pH range of 3.5 to 5.5 at 0.1 Vs^{-1} of the scan rate at the PAG/ZnO-CNTCE surface. The obtained voltammograms are shown in Figure 7(a), depicting well-defined redox peaks shifting in the negative direction with an increase in pH. The peak current intensity increased as the pH of the solution increased from 3.5 to 4.5, and thereafter it slowly decreased till pH 5.5, as depicted in Figure 7(b). Thus, pH 4.5 was chosen as the optimum pH for the further studies. The shifting of the peak in the negative direction with respect to the change in pH confirms the proton involvement in the electrochemical reaction of FA. The graph representing this can be seen in Figure 7(c), and the linear regression equation related to this is represented by Equation (4):

$$E_{pa} = -0.044\ pH + 0.562\ (R^2=0.986) \quad (4)$$

The slope value of 0.0448 V/pH, which is close to the Nernst value (0.059 V/pH), confirms that an equal number of protons and electrons are participating in the reaction. The number of protons (m) involved in the redox reaction of FA was found to be 1.62 ≈ 2, calculated from Equation (5):

$$B = \frac{-2.303mRT}{nF} \quad (5)$$

Here, B is the slope value from the graph of E_{pa} versus pH, R indicates the universal gas constant, n signifies the number of electrons, T is the temperature, and F indicates Faraday's constant.

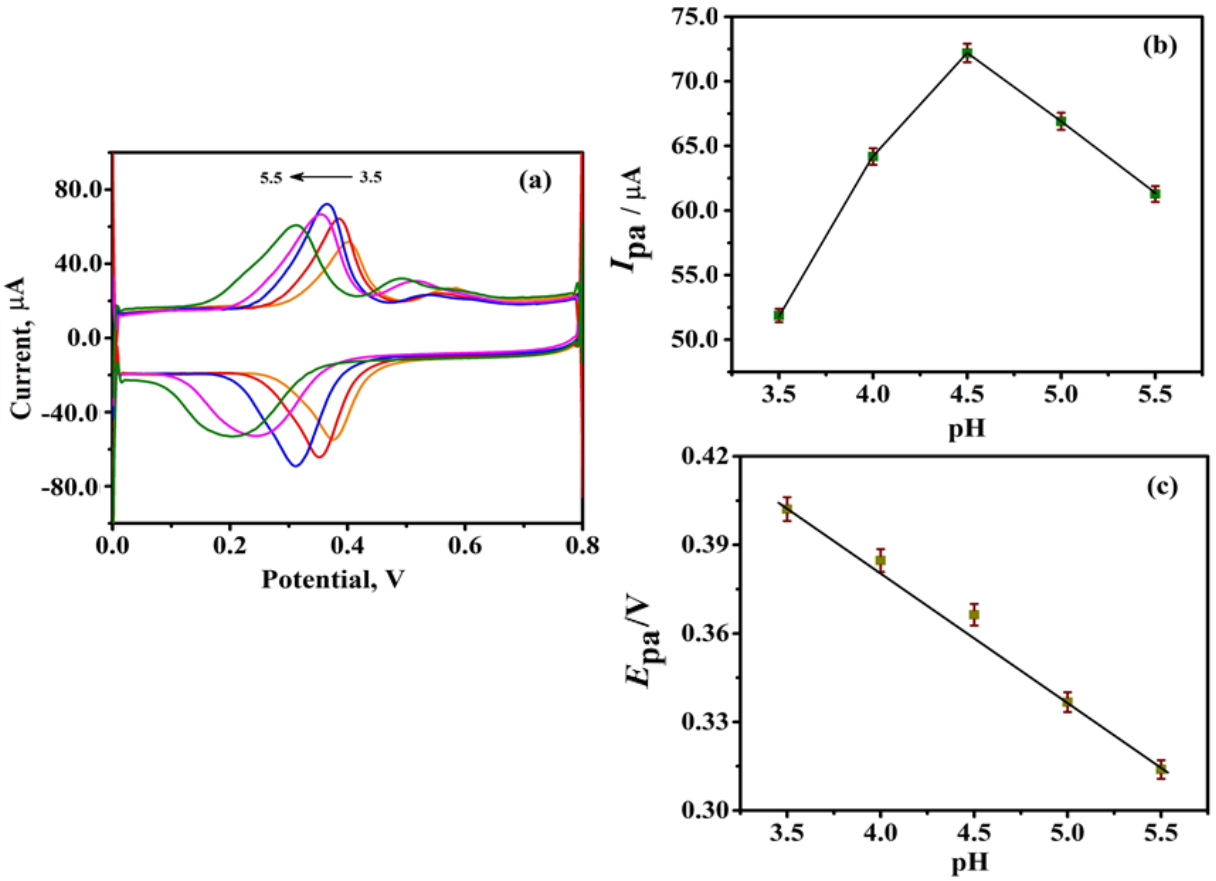

Figure 7. *(a) CVs (0.1 V s^{-1}) for 0.1 mM FA in 0.2 M PB of different pH, at the surface of PAG/ZnO-CNTCE; (b) plot of I_{pa} against pH; (c) plot of E_{pa} against pH*

Optimization of accumulation potential and time

The impact of accumulation potential on the redox behaviour of 0.1 mM FA in pH 4.5 of 0.2 M PB at PAG/ZnO-CNTCE was investigated by varying the potential in the range of 0.4 to 1.0 V. The experiment was conducted by dipping the developed electrode in pH 4.5 of 0.2 M PB containing 0.1 mM FA in different potential ranges 0.0 to 0.4 V, 0.0 to 0.5 V, 0.0 to 0.6 V, 0.0 to 0.7 V, 0.0 to 0.8 V, 0.0 to 0.9 V and 0.0 to 1.0 V. Figure 8(a) shows the CV curves of the results, and Figure 8(b) represents the graph of current against accumulation potential. Both graphs show that the maximum response was recorded in the 0.0 to 0.8 V potential range and was considered for further FA analysis. Moreover, the effect of accumulation time on the current of 0.1 mM FA was studied in the range of 0 to 100 s. Figure 8(c) depicts the CV curves, and Figure 8(d) shows the current response against time. The current increased with an increase in time up to 40 s, and thereafter the current response decreased significantly. Hence, 40 s was chosen as the optimum condition for the detection of FA at PAG/ZnO-CNTCE.

Investigation of scan rate effect

The effect of scan rate on the redox behaviour of 0.1 mM FA in pH 4.5 of 0.2 M PB was investigated in the range of 0.01 to 0.1 V s^{-1} at the surface of PAG/ZnO-CNTCE. Figure 9(a) depicts that the peak current increases with an increase in scan rate, with small shifts in oxidation peak towards positive potential and reduction peak towards negative potential. Two oxidation peaks are observed for the redox behaviour of FA. The first peak is due to the formation of diphenol, while the second peak is the result of double bond oxidation, which is present in the side chain. Furthermore, the first peak is due to the oxidation of the FA molecules in the solution, and the second peak is probably due to the oxidation of the molecules at the surface of the electrode.

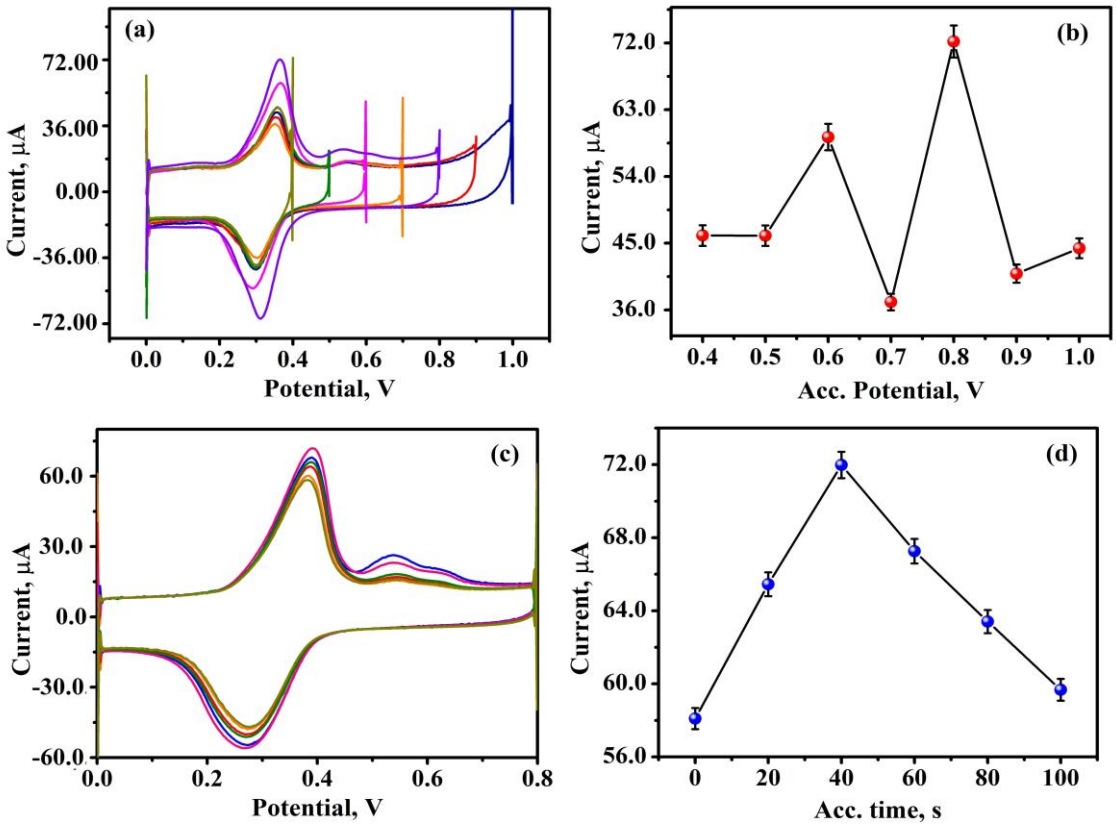

Figure. 8 *(a) CVs (0.1 V s^{-1}) for 4.5 pH of 0.2 M PB containing 0.1 mM FA at PAG/ZnO-CNTCE recorded in potential windows of 0.0 V to different accumulation potentials; (b) plot of anodic peak current versus accumulation potential; (c) CVs for the accumulation time between 0 to 100 s; (d) plot of anodic peak current against accumulation time*

A linear relation was observed between current and scan rate (ν / V s^{-1}), shown in Figure 9(b), and the logarithm of the current and the logarithm of the scan rate, shown in Figure 9(c). These indicate an adsorption-controlled process at the surface. The corresponding regressions are presented by Equations (6) to (9):

$I_{pa} = -2.2629\times10^{-6} + 0.0016\,\nu$ $R^2 = 0.9992$ (6)

$I_{pc} = -3.215\times10^{-7} + 0.001\,\nu$ $R^2 = 0.999$ (7)

$\log I_{pa} = -2.729 + 1.0059 \log \nu$ $R^2 = 0.999$ (8)

$\log I_{pc} = 2.887 + 0.986 \log \nu$ $R^2 = 0.999$ (9)

The R^2 values from Equations (6) and (7) and the slope values of Equations (8) and (9) are close to the theoretical values, indicating the surface follows an adsorption-controlled process for the detection of FA. A good linearity was observed for the relation between potential and logarithm of ν, and the corresponding regression Equations (10) and (11) related to this are presented:

$E_{pa} = 0.440 + 0.054 \log \nu$ $R^2 = 0.940$ (10)

$E_{pc} = 0.235 + 0.045 \log \nu$ $R^2 = 0.953$ (11)

The slope values of 0.0544 and 0.045 obtained from oxidation and reduction potential, respectively, were utilized for calculating the number of electrons involved in the redox reaction of FA by substituting in Laviron's Equations (12) and (13) [39]:

$$B_{pa} = \left(\frac{2.3RT}{(1-\alpha)nF} \right) \quad (12)$$

$$B_{pc} = -\left(\frac{2.3RT}{\alpha nF}\right) \quad (13)$$

The charge transfer coefficient (α) and n values were found to be 1.54 and 0.78 ≈ 1.0, respectively, which were obtained by substituting the values of B_{pa} and B_{pc} representing the slopes of equations (12) and (13). T is the temperature, R defines the universal gas constant, and F indicates Faraday's constant. The redox mechanism related to the transfer of two protons and electrons can be seen in Scheme 2 [40].

The surface coverage concentration (Γ) of the developed PAG/ZnO-CNTCE was found to be 2.683 µM cm^{-2} obtained by substituting the values of Q, the charge, and n, the number of electrons, in Equation (14) [41].

$$\Gamma = \frac{Q}{nAF} \quad (14)$$

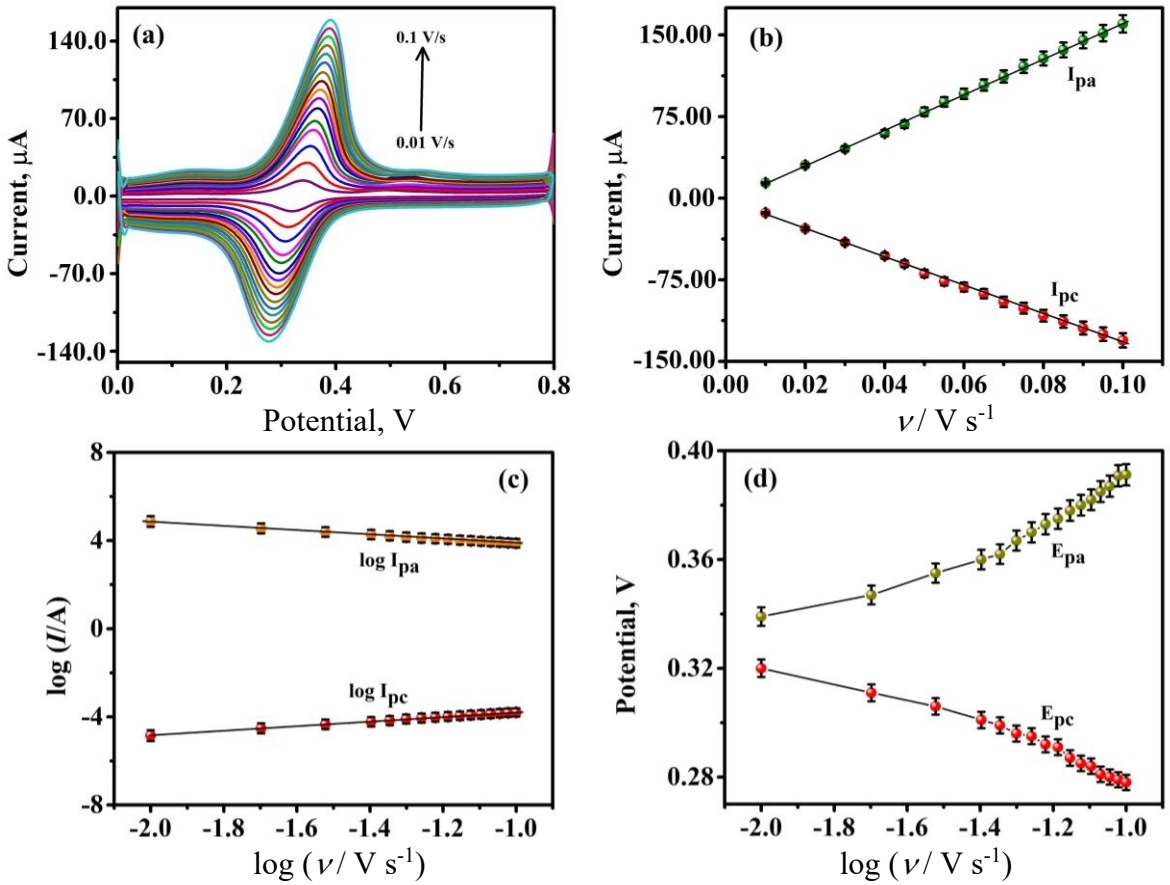

Figure 9. *(a) CVs for 0.1 mM FA in 0.2 M PB, pH 4.5, at PAG/ZnO-CNTCE for the scan rate range (ν) of 0.01 to 0.1 V s^{-1}; (b) graphs of anodic and cathodic peak currents against ν; (c) graphs of log of peak current against log ν; (d) graphs of peak potential against log ν*

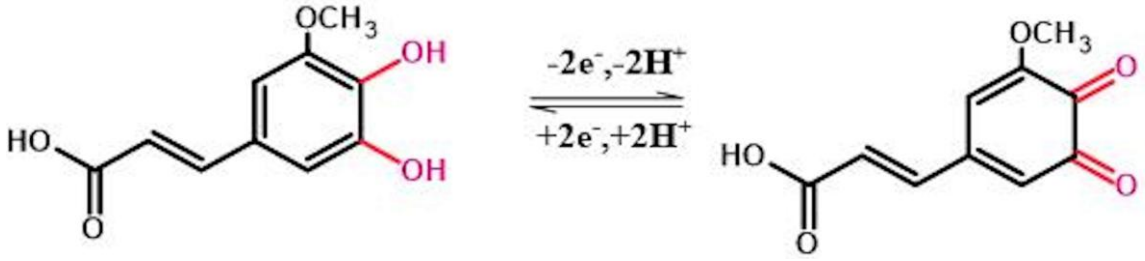

Scheme 2. *The mechanism for the redox reaction of FA*

Effect of ferulic acid concentration on PAG/ZnO-carbon nanotube electrode

The effect of FA concentration on the intensity of the redox peak current was studied by applying CV and LSV techniques, for the concentration ranging from 0.4 to 10.0 µM and 0.2 to 10.0 µM, respectively. The resulting voltammograms can be seen in Figure 10(a) and (c). The sensitivity of the peak current increased with respect to the enhanced concentration of FA, µM, but the linear dependence between the current and concentration of the analyte showed two ranges with two different slopes. Therefore, the calibration plots in Figure 10 showed two linear ranges, represented by Equations (15) to (18):

I_{pa} = -16.341 + 6.878 C_{FA} R^2 = 0.991 (CV range 1) (15)

I_{pa} = -18.528 + 49.11 C_{FA} R^2 = 0.993 (CV range 2) (16)

I_{pa} = -10.528 + 1.374 C_{FA} R^2 = 0.989 (LSV range 1) (17)

I_{pa} = -4.990 + 3.674 C_{FA} R^2 = 0.987 (LSV range 2) (18)

The LOD and LOQ were calculated by substituting the values of standard deviation (σ) and slope of the calibration plot (b) in LOD = 3σ/b and LOQ = 10σ/b [42]. The obtained LODs for CV and LSV were 0.082and 0.404 µM, respectively. The LOQs obtained for CV and LSV were 0.274 and 1.348 µM. A comparison of analytical performances, *i.e.* linear range, and LOD value of the current work with some previous works has been tabulated in Table 1.

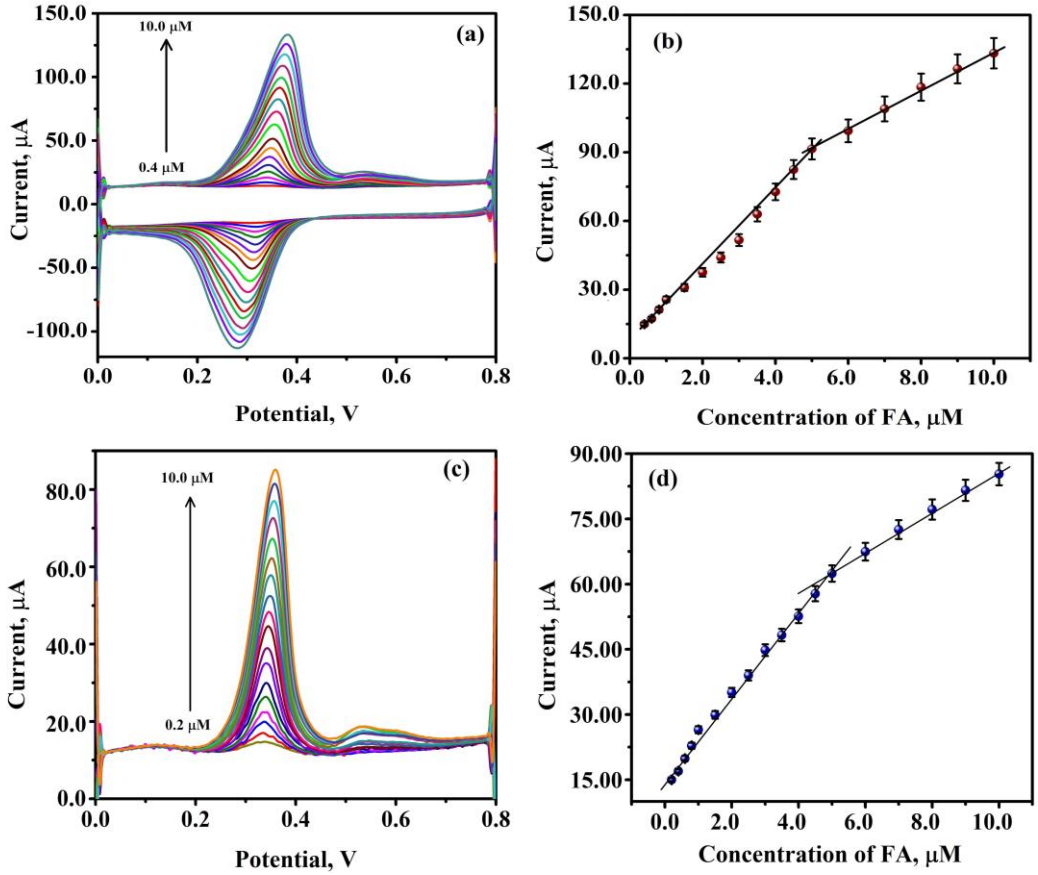

Figure 10. *(a) CVs (0.1 V s^{-1}) for PAG/ZnO-CNTCE in pH 4.5 of 0.2 M PB and FA concentrations ranging from 0.4 µM to 10.0 µM; (b) CV-based calibration plot for peak current versus concentration of FA; (c) LSVs for FA concentrations ranging from 0.2 µM to 10.0 µM; (d) LSV-based calibration plot for current versus concentration of FA*

Table 1. *Assessment of performance for FA detection of electrodes reported in the literature*

Voltametric method	Electrode	Linear range, µM	LOD, µM	Reference
CV	CNF/SPE	10 - 1000	0.778	[43]
CV	PPy-MWCNTs/GCE	3.32 - 25.9	1.17	[44]
CV	polyBCP/f-SWCNTs/GCE	0.10 - 5.0	0.072	[45]
CV	Exf-SGR/GCE	0.1 - 100	0.030	[46]
SWV	Boron-doped diamond electrode	0.15 - 0.41	0.15	[47]
CV	DDAB/nafion/CPE	2 - 1200	0.39	[48]
DPV	TiO_2/C/Au/GCE	0 - 20.0	0.016	[49]
CV	PAG/ZnO-CNTCE	0.2 - 5.0	0.082	Present work
LSV	PAG/ZnO-CNTCE	0.4 - 5.0	0.404	

Analysis of ferulic acid in the presence of hydroquinone at polyarginine modified/ZnO-carbon nanotube electrode

The electrochemical behaviour of FA (0.1 mM) and HQ (0.1 mM) in pH 4.5 of 0.2 M PB was investigated to study the selectivity of the fabricated electrode. Figure 11(a) shows the LSV response for FA and HQ at ZnO-CNTCE (curve a) and PAG/ZnO-CNTCE (curve b). No response was observed at the unmodified ZnO-CNTCE surface, but at the surface of the polymer-modified electrode, prominent current peaks of 69.57 µA and 77.72 µA are obtained for HQ and FA, respectively. The oxidation current response for both HQ and FA increased with an increase in the concentration range of 0.5 to 2.5 µM at the surface of PAG/ZnO-CNTCE in pH 4.5; the LSVs for this are depicted in Figure 11(b).

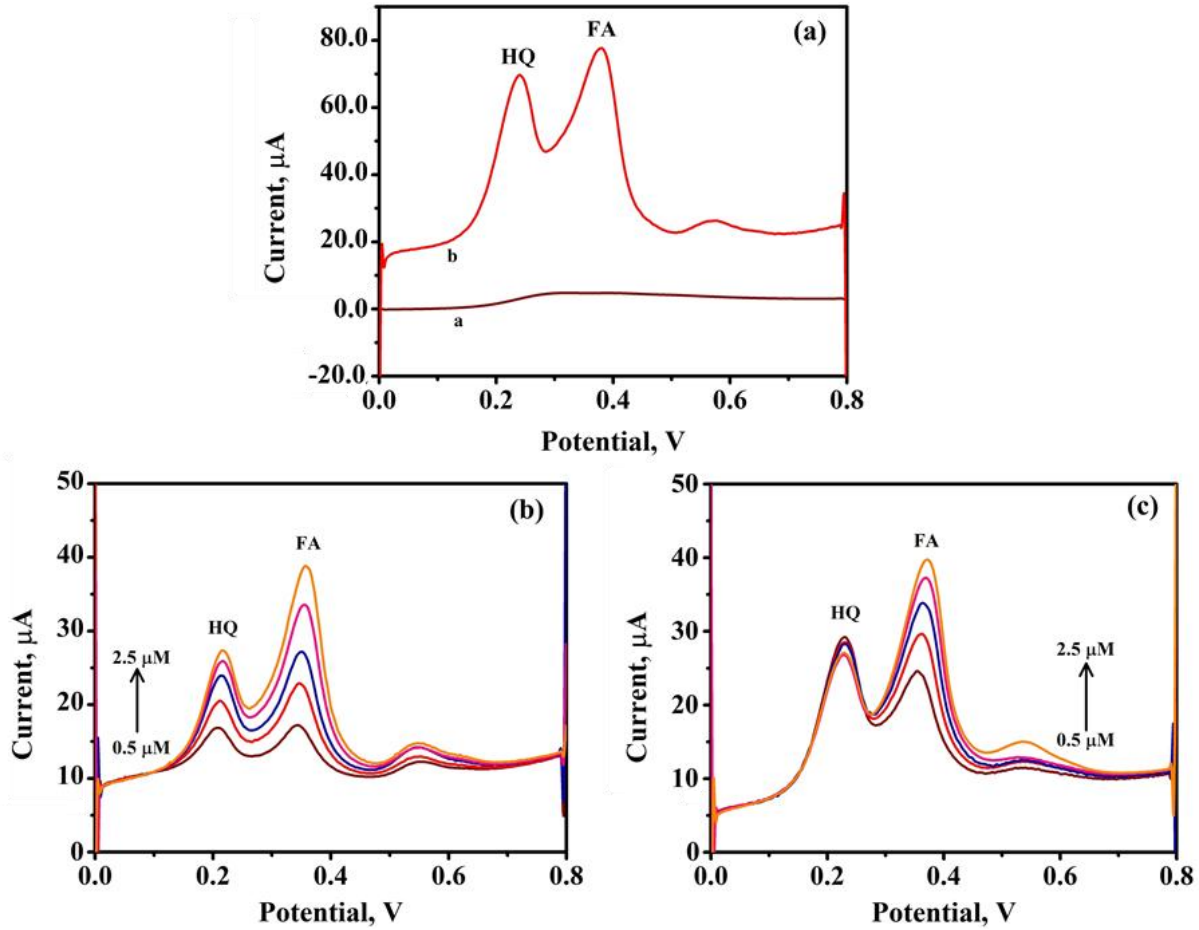

Figure 11. *(a) LSVs for HQ concentration of 0.1 mM and FA concentration of 0.1 mM at 4.5 pH of 0.2 M PB at ZnO-CNTCE (curve a) and PAG/ZnO-CNTCE (curve b); (b) LSVs for concentration variation of HQ and FA in the range 0.5 to 2.5 µM at PAG/ZnO-CNTCE; (c) LSVs for constant HQ concentration (0.5 µM) and varying FA concentration in the range 0.5 to 2.5 µM at PAG/ZnO-CNTCE*

By considering the constant concentration of HQ (0.5 µM), the concentration of FA was varied in the range of 0.5 to 2.5 µM. As seen in Figure 11(c), the current of the FA peak increased with the concentration of FA at PAG/ZnO-CNTCE, while the effect of FA concentration variation was insignificant for HQ peak current. The selectivity of the polymer-modified electrode was found to be good towards the simultaneous analysis of FA in the presence of HQ. Since both HQ and FA are widely used in cosmetics, the fabricated electrode can be utilized for differentiating the analytes.

Study of reproducibility, stability, and repeatability

The reproducibility of five different PAG/ZnO-CNTCEs was determined for the solution comprising 0.1 mM FA in 4.5 pH of 0.2 M PB, where the relative standard deviation (RSD) of 3.58 % was attained. The stability of PAG/ZnO-CNTCE for the detection of FA was investigated at an interval of 7 days by storing the electrode, and in this span, the current response decreased to 92.28 %. The repeatability study conducted for five different solutions of 0.1 mM FA for the same PAG/ZnO-CNTCE gave an RSD value of 3.54 %, suggesting good repeatability for the developed electrode. The bar graph representations of reproducibility, stability, and repeatability are shown in Figure 12.

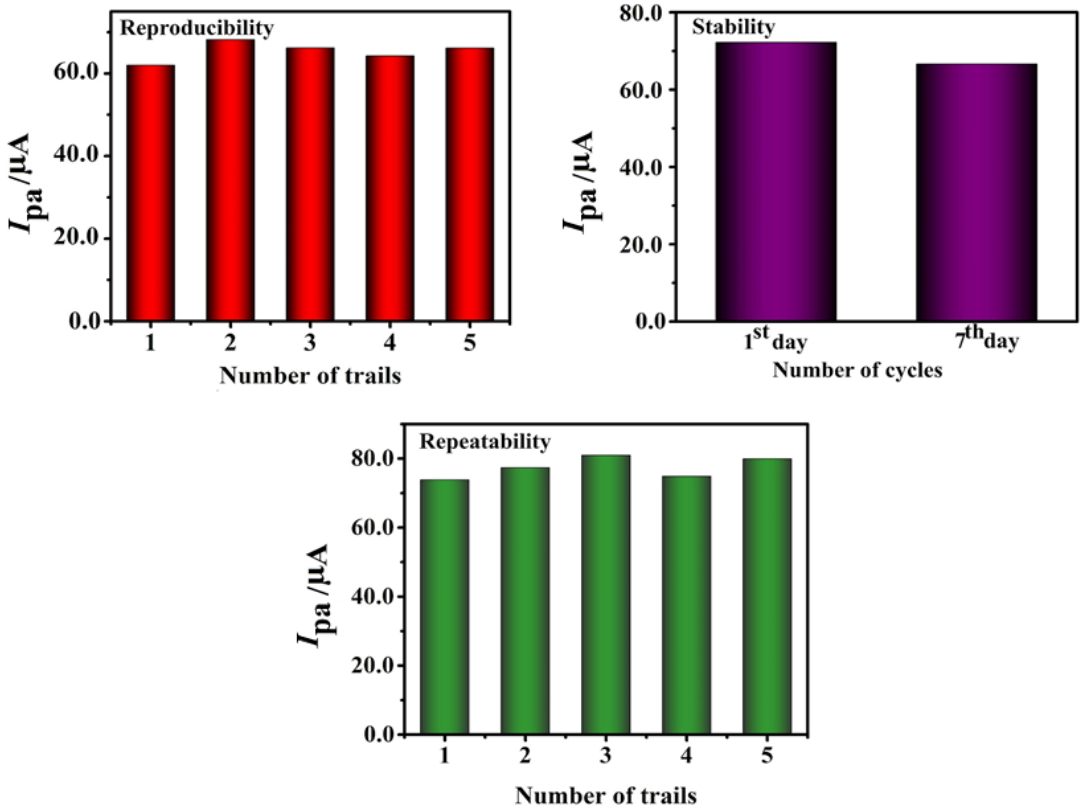

Figure 12. *Bar graph representations of reproducibility, stability, and repeatability of PAG/ZnO-CNTCE*

Interference study at polyarginine modified/ZnO-carbon nanotube electrode

The selectivity of PAG/ZnO-CNTCE for the detection of FA was verified in the presence of commonly existing foreign components. CV method was employed for the oxidation of 0.1 mM FA in pH 4.5 of 0.2 M PB at PAG/ZnO/CP-GPCE in the presence of 0.1 mM of each possible interferent, *i.e.,* uric acid (UA), tartrazine (TZ), riboflavin (RF), methyl orange (MO), adenine (AD), ascorbic acid (AA), Na^{+}, Hg^{2+}, Co^{2+}, Cd^{2+}, Ca^{2+}, As^{2+} and Mg^{2+}. The summarized results indicated that the performance of the developed sensor was not affected by the presence of different interferents, and the tolerance limit was less than ± 5 %. The graph associated with the obtained results can be seen in Figure 13, which proves that the developed electrode presents good selectivity for FA detection.

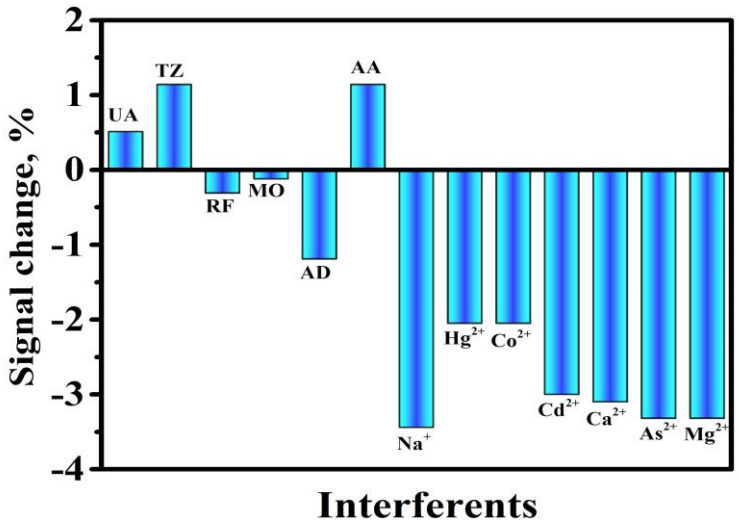

Figure 13. *Graphical representation of signal changes of 0.1 mM FA at PAG/ZnO-CNTCE versus 0.1 mM of denoted interferents*

Determination of ferulic acid in popcorn and corn powder

The fabricated PAG/ZnO-CNTCE was validated for the determination of FA in real samples like popcorn and corn powder using the CV method. The FA content was analysed in both popcorn and corn powder samples by adding successive amounts of prepared real sample solutions at pH 4.5 in the range 0.5 to 2.5 µM and the voltammograms were recorded. The calculated recovery rates are tabulated in Table 2.

Table 2. *Recovery rates of FA in real samples*

Sample	Amount added, µM	Amount found, µM	Recovery rate, %
Popcorn	0.5	0.49	98.08
	1.0	0.96	100.85
	1.5	1.44	96.63
	2.0	1.96	98.01
Corn powder	0.5	0.49	98.78
	1.0	0.99	99.08
	1.5	1.48	99.09
	2.0	1.93	96.70

Conclusion

The ZnO nanoparticles were successfully synthesized by applying a plant-mediated eco-friendly method using *Muntingia calabura* leaf extract. The surface morphology and chemical structure of the synthesized ZnO nanoparticles were analysed using XRD, EDS, and SEM images. The increase in the surface area from 0.0084 to 0.018 cm^2 for the developed PAG/ZnO-CNTCE electrode confirmed the formation of the polymer film on the surface of the bare sensor. The fabricated PAG/ZnO-CNTCE showed good sensing ability for the redox reaction of FA with the involvement of 2 protons and 2 electrons. The PAG/ZnO-CNTCE showed LOD values of 0.082 and 0.404 µM, respectively, for CV and LSV in the wide range of 0.2 to 5.0 and 0.4 to 5.0 µM. Good selectivity, sensitivity, stability, repeatability, and reproducibility make the developed electrode a most reliable sensing material for the detection of FA. The PAG/ZnO-CNTCE was successfully implemented in the simultaneous detection of FA and HQ. The applicability of the developed sensor was assessed for FA analysis in both popcorn and corn powder samples, with a recovery rate of 96.63 to 100.85 % and 96.70 to 99.09 %, respectively.

Acknowledgements: *J. G. Manjunatha gratefully acknowledge the financial support from the VGST, Bangalore under Research Project. No. VGST/K-FIST L2/2022-23/GRD-1020.*

Declaration of competing interest: *The authors declare that they have no known competing financial interests or personal relationships that could have appeared to influence the work reported in this paper.*

References

[1] D. Yoshihara, N. Fujiwara, K. Suzuki, Antioxidants: Benefits and risks for long-term health, *Maturitas* **67(2)** (2010) 103-107. https://doi.org/10.1016/j.maturitas.2010.05.001

[2] E. de Oliveira Silva, R. Batista, Ferulic Acid and Naturally Occurring Compounds Bearing a Feruloyl Moiety: A Review on Their Structures, Occurrence, and Potential Health Benefits, *Comprehensive Reviews in Food Science and Food Safety* **16(4)** (2017) 580-616. https://doi.org/10.1111/1541-4337.12266

[3] K. Zduńska, A. Dana, A. Kolodziejczak, H. Rotsztejn, Antioxidant Properties of Ferulic Acid and Its Possible Application, *Skin Pharmacology Physiology* **31(6)** (2018) 332-336. https://doi.org.10.1159/000491755

[4] S. S. Damasceno, B. B. Dantas, J. Ribeiro-Filho, Demetrius Antônio M. Araújo, J. Galberto M. da Costa, Chemical Properties of Caffeic and Ferulic Acids in Biological System: Implications in Cancer Therapy. A Review, *Current Pharmaceutical Design* **23(20)** (2017) 3015-3023. http://dx.doi.org/10.2174/1381612822666161208145508

[5] E. Girsang, I. N. Ehrich Lister, C. N. Ginting, M. Bethasari, A. Amalia, W. Widowati, Comparison of Antiaging and Antioxidant Activities of Protocatechuic and Ferulic Acids, *Molecular and Cellular Biomedical Sciences* **4(2)** (2020) 68-75. http://dx.doi.org/10.21705/mcbs.v4i2.90

[6] R. Sauce, C. Aparecida Sales de Oliveira Pinto, M. Valéria Robles Velasco, C. Rosado, A. Rolim Baby, *Ex vivo* penetration analysis and anti-inflammatory efficacy of the association of ferulic acid and UV filters, *European Journal of Pharmaceutical Sciences* **156** (2021) 105578. https://doi.org/10.1016/j.ejps.2020.105578

[7] X.-X. Zhang, D.-S. Zhao, J. Wang, H. Zhou, L. Wang, J.-L. Mao, J.-X. He, The treatment of cardiovascular diseases: a review of ferulic acid and its derivatives, *Die Pharmazie - An International Journal of Pharmaceutical Sciences* **76(2-3)** (2021) 55-60. https://doi.org/10.1691/ph.2021.0958

[8] A. S. Singer Brugiolo, A. C. Carvalho Gouveia, C. C. de Souza Alves, F. M. de Castro e Silva, É. E. de Oliveira, A. P. Ferreira, Ferulic acid supresses Th2 immune response and prevents remodeling in ovalbumin-induced pulmonary allergy associated with inhibition of epithelial-derived cytokines, *Pulmonary Pharmacology & Therapeutics* **45** (2017) 202-209. https://doi.org/10.1016/j.pupt.2017.07.001

[9] I. Antonopoulou, E. Sapountzaki, U. Rova, P. Christakopoulos, Ferulic Acid from Plant Biomass: A Phytochemical with Promising Antiviral Properties, *Frontiers in Nutrition* **8** (2022) 777576. https://doi.org/10.3389/fnut.2021.777576

[10] R. Nankar, P.K. Prabhakar, M. Doble, Hybrid drug combination: Combination of ferulic acid and metformin as anti-diabetic therapy, *Phytomedicine* **37** (2017) 10-13. https://doi.org/10.1016/j.phymed.2017.10.015

[11] C. Shi, X. Zhang, Y. Sun, M. Yang, K. Song, Z. Zheng, Y. Chen, X. Liu, Z. Jia, R. Dong, L. Cui, X. Xia, Antimicrobial Activity of Ferulic Acid Against *Cronobacter sakazakii* and Possible Mechanism of Action, *Foodborne Pathogens and Disease* **13(4)** (2016). https://doi.org/10.1089/fpd.2015.1992

[12] F.-H. Lin, J.-Y. Lin, R. D. Gupta, J. A. Tournas, J. A. Burch, M. A. Selim, N. A. Monteiro-Riviere, J. M. Grichnik, J. Zielinski, S. R. Pinnell, Ferulic Acid Stabilizes a Solution of Vitamins C and E

and Doubles its Photoprotection of Skin, *Journal of Investigative Dermatology* **125(4)** (2005) 826-832. https://doi.org/10.1111/j.0022-202X.2005.23768.x

[13] X. Huang, W. Jiang, J. Zhou, D. G. Yu, H. Liu, The Applications of Ferulic-Acid-Loaded Fibrous Films for Fruit Preservation, *Polymers* **14(22)** (2022) 4947. https://doi.org/10.3390/polym14224947

[14] N. Kumar, V. Pruthi, Potential applications of ferulic acid from natural sources, *Biotechnology Reports* **4** (2014) 86-93. https://doi.org/10.1016/j.btre.2014.09.002

[15] R. Ordoñez, L. Atarés, A. Chiralt, Multilayer antimicrobial films based on starch and PLA with superficially incorporated ferulic or cinnamic acids for active food packaging purposes, *Food Chemistry Advances* **2** (2023) 100250. https://doi.org/10.1016/j.focha.2023.100250

[16] W. Tian, G. Chen, Y. Gui, G. Zhang, Y. Li, Rapid quantification of total phenolics and ferulic acid in whole wheat using UV-Vis spectrophotometry, *Food Control* **123** (2021) 107691. https://doi.org/10.1016/j.foodcont.2020.107691

[17] X. Chen, J. Mao, F. Wen, X. Xu, Determination of Phenolic Acids in Botanical Pharmaceutical Products by Capillary Electrophoresis with Chemiluminescence Detection, *Analytical Letters* **54(5)** (2020) 817-829. https://doi.org/10.1080/00032719.2020.1783675

[18] L. Fu, Q. Chen, J. Chen, L. Ren, L. Tang, W. Shan, Magnetic carbon nanotubes-molecularly imprinted polymer coupled with HPLC for selective enrichment and determination of ferulic acid in traditional Chinese medicine and biological samples, *Journal of Chromatography B* **1180** (2021) 122870. https://doi.org/10.1016/j.jchromb.2021.122870

[19] S. S. Hingse, S. B. Digole, U. S. Annapure, Method development for simultaneous detection of ferulic acid and vanillin using high-performance thin layer chromatography, *Journal of Analytical Science and Technology* **5** (2014) 21. https://doi.org/10.1186/s40543-014-0021-6

[20] M. I. Razboršek, M. Ivanović, M. Kolar, Validated Stability-Indicating GC-MS Method for of Forced Degradation Products of Trans-Caffeic Acid and Trans-Ferulic Acid, *Molecules* **26(9)** (2021) 2475. https://doi.org/10.3390/molecules26092475

[21] P. Ebrahimi, S. A. Shahidi, M. Bijad, A rapid voltammetric strategy for determination of ferulic acid using electrochemical nanostructure tool in food samples, *Journal of Food Measurements and Characterisation* **14** (2020) 3389-3396. https://doi.org/10.1007/s11694-020-00585-z

[22] T. Zabihpour, S. A. Shahidi, H. Karimi-Maleh, A. Ghorbani-Hasan Saraei, An ultrasensitive electroanalytical sensor based on MgO/SWCNTs- 1-Butyl-3-methylimidazolium bis(trifluoromethylsulfonyl)imide paste electrode for the determination of ferulic acid in the presence sulfite in food samples, *Microchemical Journal* **154** (2020) 104572. https://doi.org/10.1016/j.microc.2019.104572

[23] N. Ebrahimi, H. A. Rafiee-Pour, E. Mahmoodi-Khaledi, Ferulic acid detection in honey using carbon paste electrode modified by C-C_3N_4/$Li_2CoMn_3O_8$ nanocomposite, *Microchemical Journal* **203** (2024) 110925. https://doi.org/10.1016/j.microc.2024.110925

[24] S. Rajendrachari, H. Arslanoglu, A. Yaras, S. M. Golabhanvi, Electrochemical Detection of Uric Acid Based on a Carbon Paste Electrode Modified with Ta_2O_5 Recovered from Ore by a Novel Method, *ACS Omega* **8(49)** (2023) 46946-46954. https://doi.org/10.1021/acsomega.3c06749

[25] S. Rajendrachari, N. Basavegowda, R. Vinaykumar, D. Narsimhachary, P. Somu, M. J. Lee, Electrocatalytic determination of methyl orange dye using mechanically alloyed novel metallic glass modified carbon paste electrode by cyclic voltammetry, *Inorganic Chemistry Communications* **155** (2023) 111010. https://doi.org/10.1016/j.inoche.2023.111010

[26] R. S. Mahale, V. Rajashekar, S. Vasanth, S. P. Chikkegowda, S. Rajendrachari, V. Mahesh, Fabrication of Mechanically Alloyed Super Duplex Stainless Steel Powder-Modified Carbon Paste Electrode for the Determination of Methylene Blue by the Cyclic Voltammetry

Technique, *ACS Omega* **9(9)** (2024) 10660-10670. https://doi.org/10.1021/acsomega.3c09163

[27] B. Kanthappa, J. G. Manjunatha, S. A. Aldossari, S. Mohammad, C. Raril, Sensing of paracetamol in the presence of dopamine using an electrochemically polymerized l-alanine layered carbon nanotube sensor, *Journal of Materials Science: Materials in Electronics* **35** (2024) 768. https://doi.org/10.1007/s10854-024-12535-2

[28] P. Xiao, F. Zhao, B. Zeng, Voltammetric determination of quercetin at a multi-walled carbon nanotube paste electrode, *Microchemical Journal* **85(2)** (2007) 244-249. https://doi.org/10.1016/j.microc.2006.06.004

[29] P. Kannan, G. Maduraiveeran, Metal Oxides Nanomaterials and Nanocomposite-Based Electrochemical Sensors for Healthcare Applications, *Biosensors* **13(5)** (2023) 542. https://doi.org/10.3390/bios13050542

[30] S. Devaraj, J. G. Manjunatha, S. A. Aldossari, S. Mohammad, N. Ataollahi, Analysis of Brucine using Poly(L-Arginine) modified biosynthesized CuO nanoparticle composite sensor, *Journal of Taibah University for Science* **18(1)** (2024) 2425082. https://doi.org/10.1080/16583655.2024.2425082

[31] S. Rajendrachari, H. Arslanoglu, A. Yaras, S.M. Golabhanvi, Electrochemical Detection of Uric Acid Based on a Carbon Paste Electrode Modified with Ta_2O_5 Recovered from Ore by a Novel Method, *ACS Omega* **8 (49)** (2023) 46946-46954. https://doi.org/10.1021/acsomega.3c06749

[32] S. Suvetha, G. Muruganandam, G. Hariharan, N. Nesakumar, A. J. Kulandaisamy, J. B. Balaguru Rayappan, B. M. Gunasekaran, Electrochemical investigation on calcium ion sensing and steady-state diffusion analysis using zinc oxide modified glassy carbon electrode, *Measurement* **221** (2023) 113511. https://doi.org/10.1016/j.measurement.2023.113511

[33] S. Rajendrachari, P. Taslimi, A. C. Karaoglanli, O. Uzun, E. Alp, G. K. Jayaprakash, Photocatalytic degradation of Rhodamine B (RhB) dye in waste water and enzymatic inhibition study using cauliflower shaped ZnO nanoparticles synthesized by a novel One-pot green synthesis method, *Arabian Journal of Chemistry* **14(6)** (2021) 103180. https://doi.org/10.1016/j.arabjc.2021.103180

[34] S. Rajendrachari, E. Altaş, A. Erdogan, Y. Küçük, M. Sabri Gök, F. Khosravi, Electrochemical determination of dopamine by poly (methyl orange) shape memory alloy modified carbon paste electrode, *Inorganic Chemistry Communications* **167** (2024) 112826. https://doi.org/10.1016/j.inoche.2024.112826

[35] Y. Yi, Z. Mao, L. Luo, B. Wang, Z. Zhao, Z. Hao, A. Luo, Enhanced performance of microbial electrochemical systems prepared with in situ electropolymerization of L-arginine-modified carbon cloth, *Journal of Cleaner Production* **392** (2023) 136244. https://doi.org/10.1016/j.jclepro.2023.136244

[36] R. Shashanka, Investigation of optical and thermal properties of CuO and ZnO nanoparticles prepared by *Crocus Sativus* (Saffron) flower extract, *Journal of the Iranian Chemical Society* **18** (2021) 415-427. https://doi.org/10.1007/s13738-020-02037-3

[37] J. G. Manjunatha, A surfactant enhanced graphene paste electrode as an effective electrochemical sensor for the sensitive and simultaneous determination of catechol and resorcinol, *Chemical Data Collection* **25** (2020) 100331. https://doi.org/10.1016/j.cdc.2019.100331

[38] B.M. Amrutha, J.G. Manjunatha, N. Hareesha, A.M. Tighezza, M.D. Albaqami, M. Sillanpää, Electrochemical polymerisation of glutamic acid on the surface of graphene paste electrode for the detection and quantification of rutin in food and medicinal samples, *Diagnostics* **12** (2022) 3113. https://doi.org/10.3390/diagnostics12123113

[39] E. Laviron, Theoretical study of a reversible reaction followed by a chemical reaction in thin layer linear potential sweep voltammetry, *Journal of Electroanalytical Chemistry and Interfacial Electrochemistry* **39** (1972) 1-23. https://doi.org/10.1016/s0022-0728(72)80472-8
[40] A. V. Bounegru, C. Apetrei, Development of a Novel Electrochemical Biosensor Based on Carbon Nanofibers-Gold Nanoparticles-Tyrosinase for the Detection of Ferulic Acid in Cosmetics, *Sensors* **20** (2020) 6724. https://doi.org/10.3390/s20236724
[41] S. Battira Madappa, J. G. Manjunatha, M. Karnayana, S. Mahmoud Osman, S. Patra, A surface-modified graphene - carbon-based composite sensor for the voltammetric assessment of pyridoxine in food and pharmaceutical samples, *Journal of Taibah University for Science* **18(1)** (2024) 2359209. https://doi.org/10.1080/16583655.2024.2359209
[42] I. G. David, D. E. Popa, M. Buleandra, S. N. Codreanu, L. Croitoru, L. A. Iordache, H. Noor, Voltammetric Investigation of Ferulic Acid at Disposable Pencil Graphite Electrode, *Micromachines* **14** (2023) 1951. https://doi.org/10.3390/mi14101951
[43] A. V. Bounegru, C. Apetrei, Simultaneous Determination of Caffeic Acid and Ferulic Acid Using a Carbon Nanofiber-Based Screen-Printed Sensor, *Sensors* **22(13)** (2022) 4689. https://doi.org/10.3390/s22134689
[44] R. Abdel-Hamid, E. F. Newair, Polypyrrole-Multiwalled Carbon Nanotubes Modified Electrode with Sample Application, *Nanomaterials* **5(4)** (2015) 1704-1715. https://doi.org/10.3390/nano5041704
[45] G. Ziyatdinova, A. Zhupanova, R. Davletshin, Simultaneous Determination of Ferulic Acid and Vanillin in Vanilla Extracts Using Voltammetric Sensor Based on Electropolymerized Bromocresol Purple, *Sensors* **22(1)** (2022) 288. https://doi.org/10.3390/s22010288
[46] L. Măgeruşan, F. Pogăcean, M. L. Soran, Stela-Maria Pruneanu, Graphene-Based Electrochemical Sensing Platform for Rapid and Selective Ferulic Acid Quantification, *International Journal of Molecular Sciences* **24(23)** (2023) 16937. https://doi.org/10.3390/ijms242316937
[47] P. T. Pınar, Hemn A. H. Barzani, H. S. Ali, Yavuz Yardım, Quantification of ferulic acid using square-wave voltammetric method at an unmodified boron-doped diamond electrode, *Chemical Monthly* **154** (2023) 1225-1233. https://doi.org/10.1007/s00706-023-03126-8
[48] L. Luo, X. Wang, Q. Li, Y. Ding, J. Jia, D. Deng, Voltammetric Determination of Ferulic Acid by Didodecyldimethyl-ammonium Bromide/Nafion Composite Film-modified Carbon Paste Electrode, *Analytical Science* **26** (2010) 907-911. https://doi.org/10.2116/analsci.26.907
[49] G. Li, S. Liu, Y. Liu, X. Pang, M. Li, Y. Gong, Y. Wu, X. Guo, Au-doped nanostructured TiO_2/C material derived from MIL-125 as a highly sensitive electrochemical sensor for ferulic acid, *Journal of Coordination Chemistry* **76** (2023) 1007-1019. https://doi.org/10.1080/00958972.2023.2221375